Supporting Information

Superparamagnetism of Green Emissive Cs_4PbBr_6 Zero-Dimensional Perovskite Crystals

Ji-Hyun Cha,[a] *Hyun-Jong Lee,*[a,b] *Sun Ha Kim,*[c] *Kyoung Chul Ko,*[d] *Byoung Jin Suh,*[e] *Oc Hee Han,*[c] *and Duk-Young Jung*[a,b,*]

[a]Department of Chemistry, Sungkyunkwan University, Suwon, Gyeonggi-do 16419, Republic of Korea

[b]Sungkyunkwan Advanced Institute of Nano Technology, Sungkyunkwan University, Suwon, Gyeonggi-do 16419, Republic of Korea

[c]Western Seoul Center, Korea Basic Science Institute, Seoul 03759, Republic of Korea

[d]Department of Chemistry Education, Chonnam National University, Gwangju 61186, Republic of Korea

[e]Department of Physics, The Catholic University of Korea, Bucheon 16444, Republic of Korea

EXPERIMENTAL METHODS

General methods

Cesium (I) bromide (CsBr, 99.9%), lead (II) bromide ($PbBr_2$, 99.9%), hydrobromic acid (HBr, 48%), γ-butyrolactone (GBL, 99%) dimethyl sulfoxide (DMSO, 99.8%), dimethylformamide (DMF, 99.5%) and dichloromethane (DCM, 99.8%) were purchased from Sigma-Aldrich and used without further purification. G416 and N416 crystals were grown by a slow temperature cooling method. The crystals were evaluated by PXRD, Raman spectroscopy, field emission scanning electron microscopy (FE-SEM), and EDS. PXRD was employed using an X-ray diffractometer (Rigaku, Ultima IV) in the $\theta - 2\theta$ scanning mode at 40 kV and 30 mA using CuKa radiation (λ = 1.5405 Å). Raman spectroscopy measurements (WITec, ALPHA 300) were carried out using a 633 nm laser source at room temperature. The surface morphology and compositional analysis of the crystals were evaluated using a FE-SEM (JEOL, JSM-7100F) attached EDS system. Reflectance UV-vis spectra were obtained with a Shimadzu UV-3600 UV/Vis-near-IR spectrophotometer using an ISR-3100 integrating sphere and barium sulfate as a standard.

Synthetic procedure

For the growth of G416 crystals, 1.2 mmol of CsBr and 0.3 mmol of $PbBr_2$ were simultaneously dissolved into 6 ml of a DMSO solution at 90°C with magnetic stirring. After 1 hour, a clear precursor solution was prepared and then 3 ml of HBr was added into the precursor solution. The final solution was stored in the slow cooling camber and the temperature was decreased at a cooling rate of 2 °C/hour. After the solution was cooled down to room temperature, we collected the G416 crystals from the cultivation solution by washing with DMF and DCM solvents sequentially. N416 crystals were grown by following a previous report.[1] 0.05 mol of CsBr was dissolved in 10 ml of deionized water and 0.16 mmol of $PbBr_2$ was dissolved in 1 ml of HBr at 90°C. After 1 hour, the two solutions were mixed and then stored in the cooling camber. After the solution was cooled down to room temperature, we separated the crystals from the cultivation solution by washing with GBL, DMF, and DCM solvents.

Characterization

SC-XRD data of G416 and N416 was obtained at the 2D-SMC beam line (2019-3rd-2D-020) at the Pohang Accelerator Laboratory (PAL), Korea. Diffraction data was corrected using a

CCD detector (Rayonix, MX225-HS). HKL3000sm was used for unit cell refinement. The crystal structures were solved using the SHELXLE program package containing SHELX-L (version 2018/3).

The magnetization measurements were carried out using MPMS (Quantum Design) at the Korea Basic Science Institute (KBSI). Measurements were performed on the powdered crystal samples that were potted into gelatin capsules. The magnetization−magnetic field (M-H) dependence was obtained in the range of −5 T to +5 T at room temperature and 4.2 K. All of the magnetization data was corrected for the diamagnetic background from gelatin capsules.

The ^{133}Cs MAS NMR data of perovskite crystals were obtained using 4 mm outer-diameter zirconia rotors at a 10 kHz spinning rate on a Bruker AVANCE II^{+} 400 MHz NMR spectrometer equipped with a 9.4 T wide-bore magnet. The ^{133}Cs MAS NMR experiments were performed at a radio frequency of 52.49 MHz with a 1.6 μs excitation pulse length and 100 s pulse repetition delay time when the 90° pulse length measured using CsCl powder was 5.2 μs. The MAS NMR signal of CsCl powder acquired at room temperature was used as an external chemical shift reference for the ^{133}Cs chemical shift. The relative population of each site, chemical shifts, and line widths were obtained from the spectral simulation.

In order to analyze the effect of Br vacancies on Cs_4PbBr_6 perovskite, the DFT calculations were performed within periodic boundary conditions. The N416 single unit cell and the defected N416 crystal structure possessing one Br vacancy (D-N416-V_{Br}) were fully optimized with relaxation of both nucleus positions and lattice parameters. For geometrical optimization calculations, the Perdew–Burke–Ernzerhof (PBE)/light-tier-1 level of theory with a 7×7×7 Monkhorst-Pack mesh of *k*-points was used, and the convergence criteria was set to 0.01 eV/Å. With consideration of heavy metal atoms in Cs_4PbBr_6 perovskite, relativistic effects were treated at the zeroth order regular approximation (ZORA) level scale.[2] To obtain more reliable electronic structures, the SOC was included for the single point calculations with the optimized unit cells at the same level of theory. Finally, the optimized lattice parameters, the Mulliken atomic charges and partial DOS, were analyzed for N416 and D-N416-V_{Br}. All DFT calculations were carried out using FHI-aims code. [3]

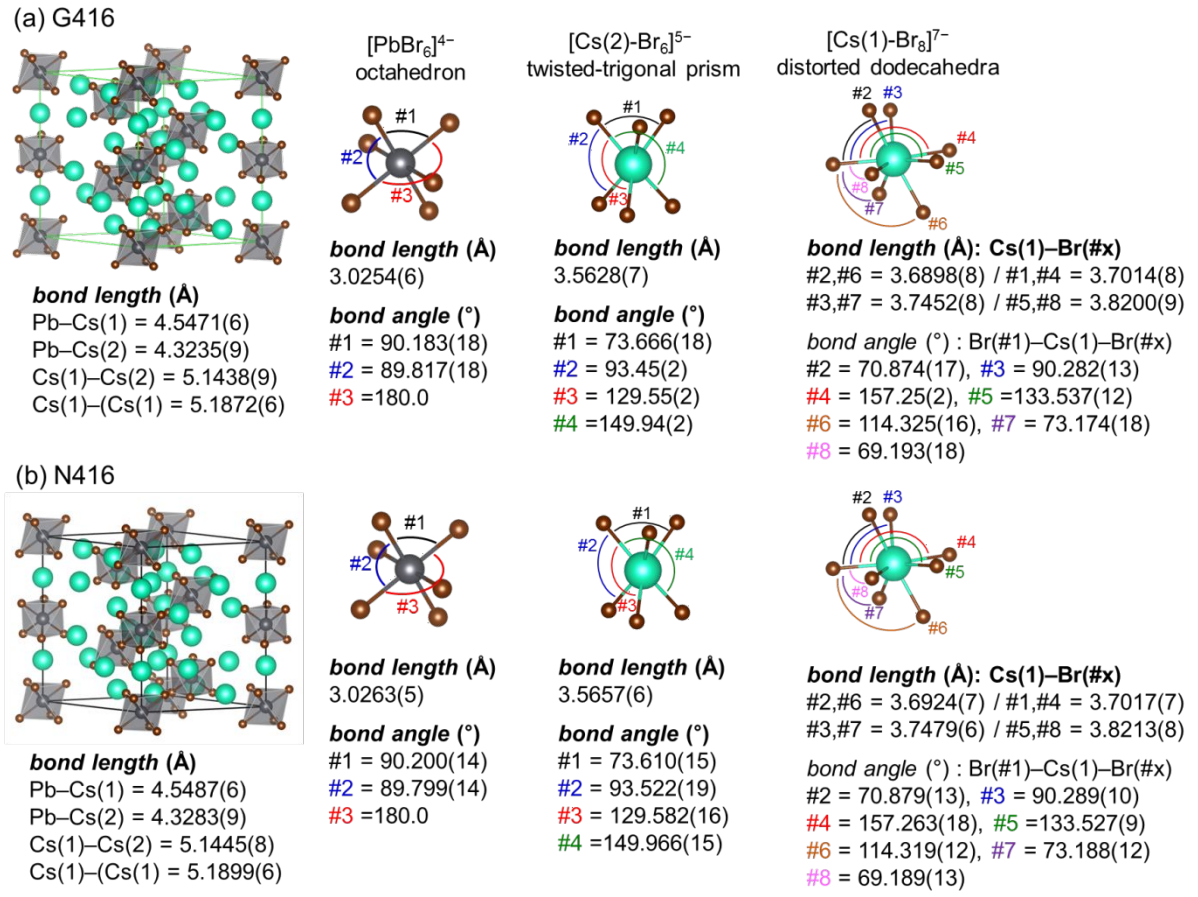

Figure S1. Details of the bond distance and angle for (a) G416 and (b) N416 crystals refined from SC-XRD results.

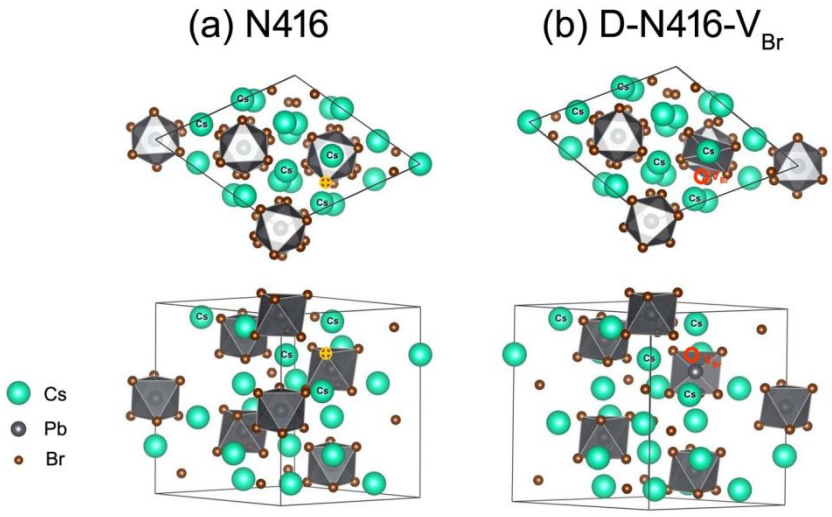

Figure S2. The optimized structures of (a) N416 and (b) D-N416-V_{Br} according to top view (top) and side view (bottom). The Br vacancy sites (red circle) of D-N416-VBr model structure is prepared by removing the selected Br atom (yellow wheel cross) in N416 unit cell.

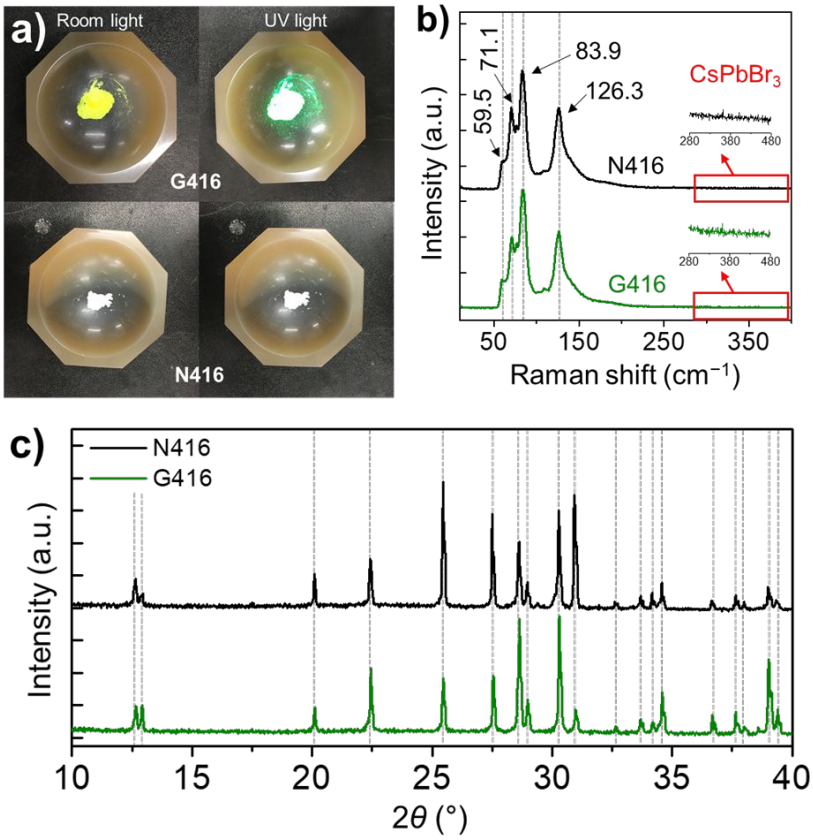

Figure S3. (a) photographs of G416 and N416 powders after grinding each crystal under ambient atmosphere. There are no changes in its color and PL emission under room and UV light. (b) Raman spectra of G416 (green line) and N416 (black line) crystals. Gray dashed lines show the center of each peak and the numbers are the Raman shift values for individual peaks. The insets in (a) show magnified spectra in red boxes. (c) PXRD patterns of G416 and N416 samples. To identify the bulk impurities in the products, the patterns are corrected by using powders obtained by grinding of crystal grown in the same batch, respectively.

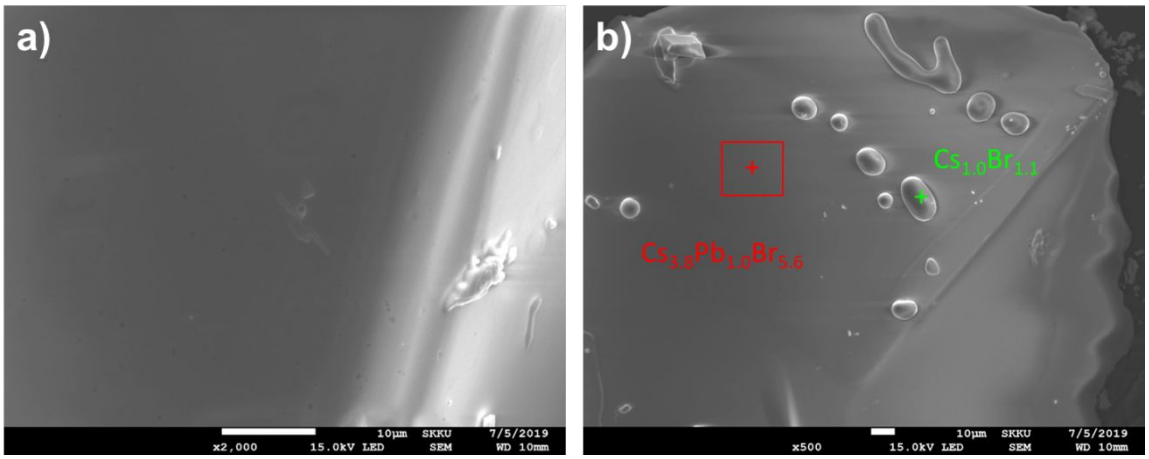

Figure S4. SEM image of (a) G416 and (b) N416 crystal surface. The G416 crystal has a smooth surface but N416 has small clusters on the surface with about 10 μm of size. A chemical formula of clusters on the N416 surface was $Cs_{1.0}Br_{1.1}$, which was carried out EDS analysis. The chemical formulas were obtained by EDS analysis with point detection mode. Quantitative analyses of G416 by energy-dispersive X-ray spectroscopy (EDS) were performed to characterize the purity of the prepared crystals of which Cs:Pb:Br composition was 3.8(3):1.03(6):6.1(3), in accordance with the ideal stoichiometry of 4:1:6. The N416 crystal has the Cs:Pb:Br ratio of 3.9(2):1.07(5):5.9(2) confirmed by EDS analysis, which is a similar composition to the G416 crystals.

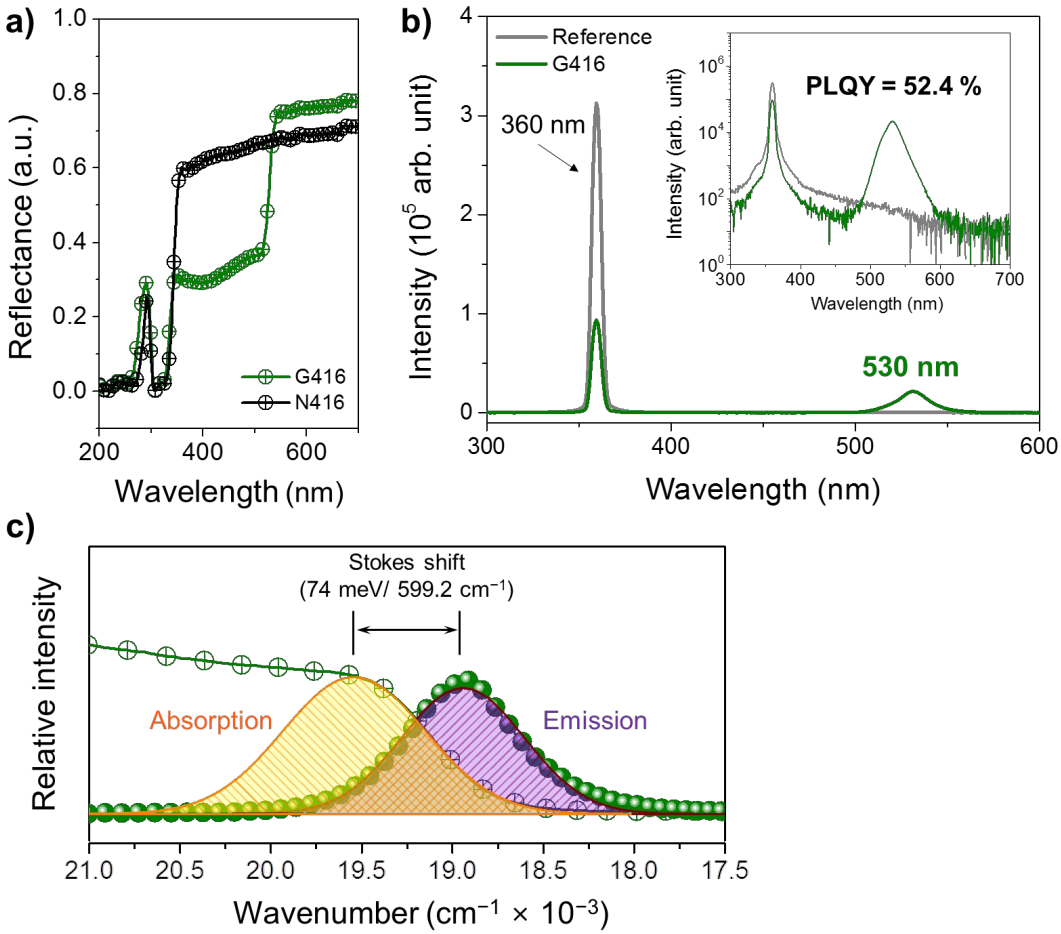

Figure S5. (a) Reflectance G416 (green line) and N416 (black line) crystals. (b) PLQY spectra of G416 crystal (gray line: reference, green line: emission spectrum from G416) (c) Absorption and emission spectra of G416 fitted with deconvoluted peaks (yellow area: absorption, purple area: emission) by using Gaussian function.

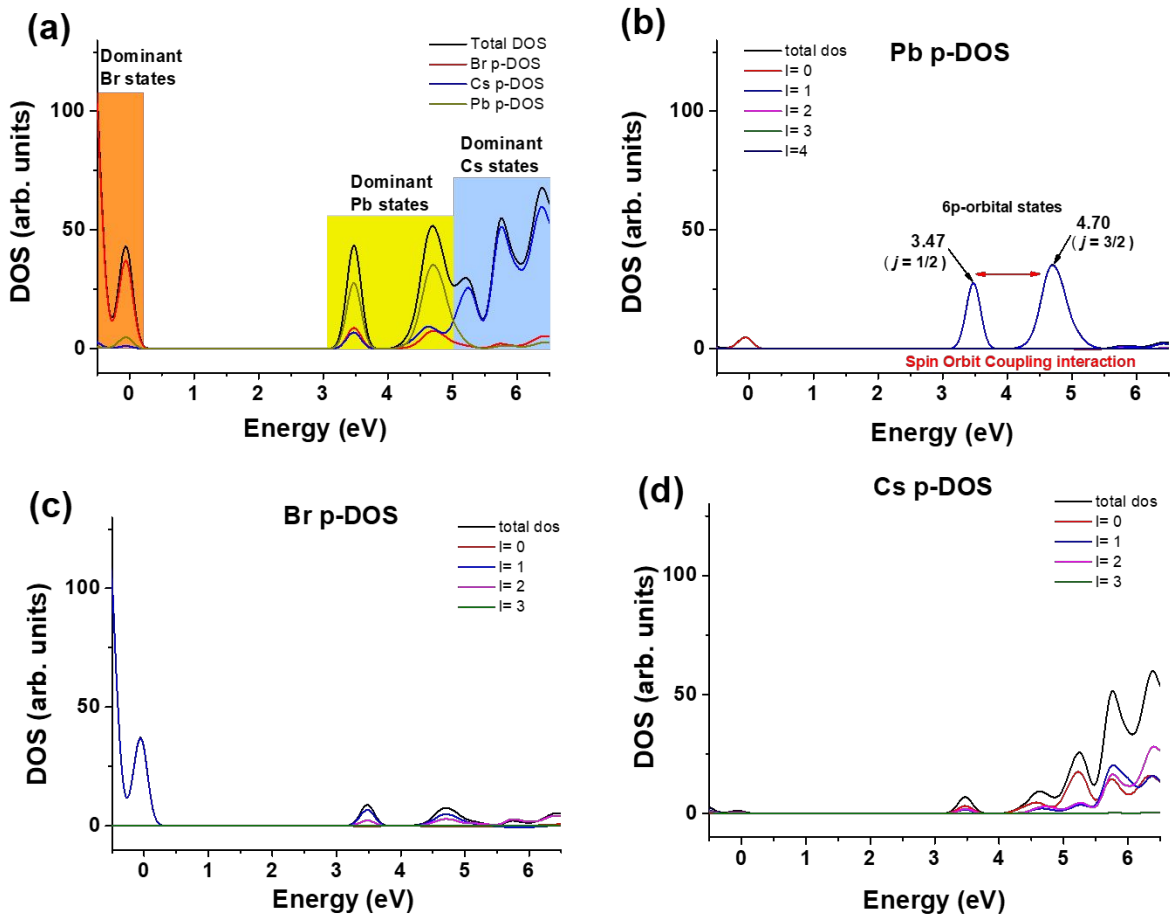

Figure S6. (a) The calculated atom-projected and angular-momentum resolved partial density of states (p-DOS) of (b) Pb, (c) Br, and (d) Cs atoms for N416 including spin-orbit coupling (SOC).

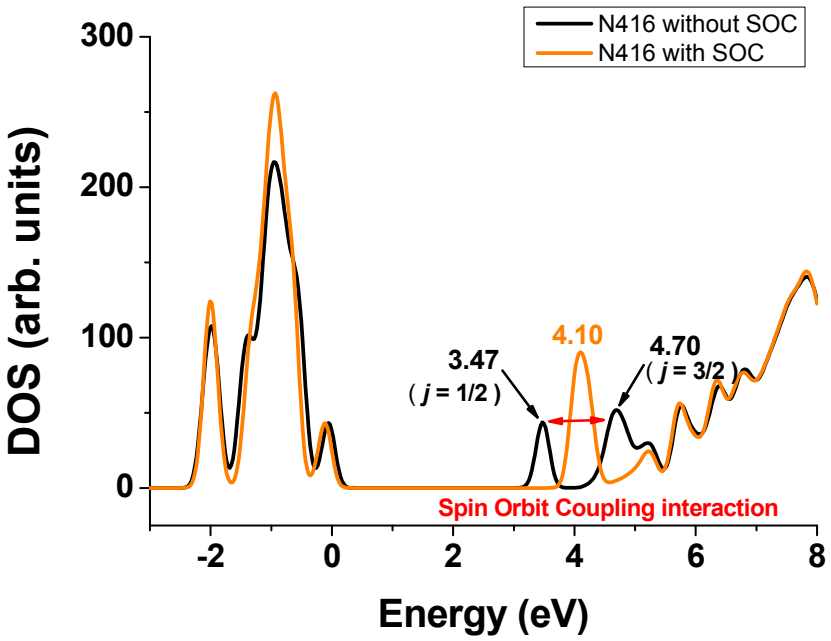

Figure S7. The calculated density of state (DOS) for N416 with (orange line) or without (black line) spin-orbit coupling (SOC). The calculated two states at 3.47 eV and 4.70 eV in DOS plots would be generated from the energy splitting due to the spin-orbit coupling (SOC) described by j=1/2 and j=3/2. (s=1/2 and l=1) The ratio of the number of degenerated states between j=1/2 level and j=3/2 level would be 1/2. In this regard, in experimental optical absorption spectra (**Figure 4b**) two peaks of 3.86 eV and 4.03 eV having 1.62 area ratio could be associated Pb p-orbital states split by spin-orbit interaction. However, the theoretical spin-orbit interaction estimated from the energy difference between two states corresponding to j=1/2 and j=3/2 (1.23 eV) are much stronger than experimental one (0.2 eV). Additionally, similar photoluminescence quantum yield (PLQY) measured with 3.86 eV and 4.03 eV for excitation light energies also support that the 3.47 eV and 4.70 eV states in calculated DOS would correspond to the 3.86 eV and 4.03 eV peaks in experimental optical absorption spectra, respectively.

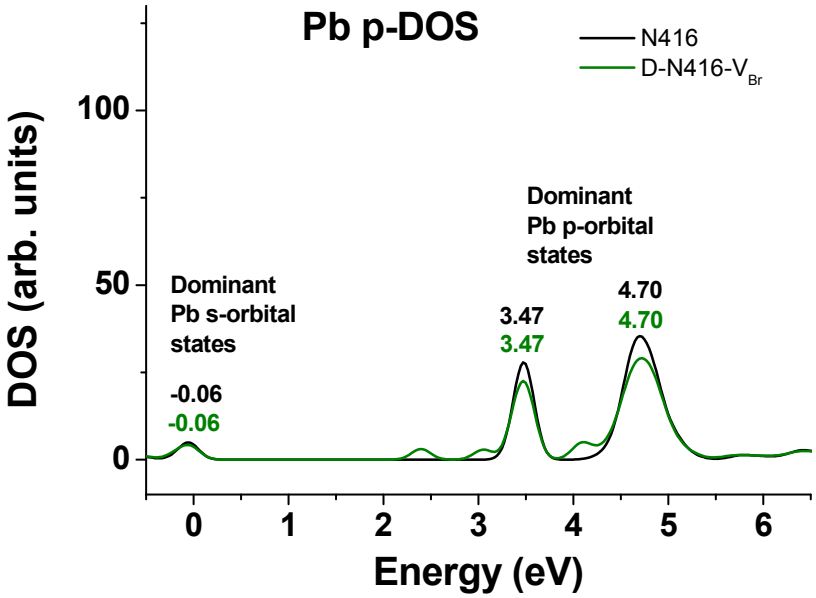

Figure S8. The comparison of calculated atom-projected (top) and angular-momentum resolved (bottom) partial density of states (p-DOS) for Pb atoms between N416 (black line) and D-N416-V_{Br} (green line).

Table S1. Crystal information and structure refinement for G416 and N416 single crystals.

Sample name	G416	N416
Temperature	300 K	
Unit cell	rhombohedral	
Space group	*R*3c	
a (Å)	13.7120(19)	13.7149(19)
b (Å)	13.7120(19)	13.7149(19)
c (Å)	17.294(4)	17.313(3)
α (°)	90	90
β (°)	90	90
γ (°)	120	120
V (Å^3)	2816.0(10)	2820.3(10)
Z	6	
Agreement factor	R_1=3.4%, wR_2=8.4%, GooF=1.123	R_1= 3.6%, wR_2=9.00%, GooF=1.127

Table S2. The calculated lattice parameters (*a*, *b*, *c, α, β* and *γ*) and unit-cell volumes of stoichiometric N416 crystal structure and defected N416 crystal structure possessing a one Br vacancy (D-N416-V_{Br}).

	a (Å)	*b* (Å)	*c* (Å)	*α* (°)	*β* (°)	*γ* (°)	Volume (Å^3)
N416	13.995	13.993	17.529	90.028	89.984	119.983	2973.263
D-N416-V_{Br}	14.002	13.992	17.497	89.862	89.836	120.051	2967.156

Table S3. ^{133}Cs MAS NMR parameters of the G416 and N416 crystals.

Crystal	Chemical shift (ppm)			FWHM (ppm)			Peak area (%)		
	peak 1	peak 2	peak 3	peak 1	peak 2	peak 3	peak 1	peak 2	peak 3
G416	−1	119	−11	6.8	10.2	7	76	22	2
N416	−2	118	−11	6.5	92	5	77	22	1

Table S4. The calculated Mulliken atomic charges (in *e*) of five Cs atoms directly adjacent to the Br vacancy site between N416 and D-N416-V_{Br} and their differences.

	N416	D-N416-V_{Br}	Differences
Cs atoms	0.7511	0.7342	-0.017
	0.7495	0.7377	-0.012
	0.7511	0.7316	-0.019
	0.7513	0.7258	-0.025
	0.7122	0.6996	-0.013

Table S5. Parameters for Gaussian fitting* of absorption and emission spectra of G416 crystal.

Parameter	Absorption		Emission	
	Value (cm^{-1})	Standard Error	Value (cm^{-1})	Standard Error
y_0	0	0	0	0
x_{cnter}	19541.40	10.9	18942.16	1.81
Area	502.24	12.1	398.40	1.85
FWHM	921.66	15.6	796.21	4.27

*Gaussian function: $y = y_0 + (A/(w\times\sqrt{(\pi/2)}))*\exp(-2\times((x-x_c)/w)^2)$

REFERENCES

(1) Zhang, Z.; Zhu, Y.; Wang, W.; Zheng, W.; Lin, R.; Li, X.; Zhang, H.; Zhong, D.; Huang, F. Aqueous Solution Growth of Millimeter-Sized Nongreen-Luminescent Wide Bandgap Cs_4PbBr_6 Bulk Crystal. *Cryst. Growth Des.* **2018**, *18* (11), 6393–6398.

(2) Huhn, W. P.; Blum, V. One-Hundred-Three Compound Band-Structure Benchmark of Post-Self-Consistent Spin-Orbit Coupling Treatments in Density Functional Theory. *Phys. Rev. Materials* **2017**, *1* (3), 033803–033818.

(3) Blum, V.; Gehrke, R.; Hanke, F.; Havu, P.; Havu, V.; Ren, X.; Reuter, K.; Scheffler, M. Ab Initio Molecular Simulations with Numeric Atom-Centered Orbitals. *Computer Physics Communications* **2009**, *180* (11), 2175–2196.